



# Identification of a Six-Gene Prognostic Signature Characterized by Tumor Microenvironment Immune Profiles in Clear Cell Renal Cell Carcinoma

Lu Zhang<sup>1</sup>, Jianlong Li<sup>2</sup>, Mengzhao Zhang<sup>1</sup>, Lu Wang<sup>1</sup>, Tao Yang<sup>1</sup>, Qiuya Shao<sup>1</sup>, Xiao Liang<sup>1</sup>, Minghai Ma<sup>1</sup>, Nan Zhang<sup>1</sup>, Minxuan Jing<sup>1</sup>, Rundong Song<sup>1</sup> and Jinhai Fan<sup>1,3\*</sup>

<sup>1</sup>Department of Urology, the First Affiliated Hospital of Xi'an Jiaotong University, Xi'an, China, <sup>2</sup>Department of Urology, Xi'an NO.3 Hospital, the Affiliated Hospital of Northwest University, Xi'an, China, <sup>3</sup>Oncology Research Lab, Key Laboratory of Environment and Genes Related to Diseases, Ministry of Education, Xi'an, China

## OPEN ACCESS

### Edited by:

Can Yang,

Hong Kong University of Science and Technology, Hong Kong SAR, China

### Reviewed by:

Natasha Andressa Jorge,

Leipzig University, Germany

Qianqian Shi,

Huazhong Agricultural University, China

### \*Correspondence:

Jinhai Fan

jinhai029@126.com

### Specialty section:

This article was submitted to Computational Genomics, a section of the journal *Frontiers in Genetics*

Received: 11 June 2021

Accepted: 20 October 2021

Published: 18 November 2021

### Citation:

Zhang L, Li J, Zhang M, Wang L, Yang T, Shao Q, Liang X, Ma M, Zhang N, Jing M, Song R and Fan J (2021) Identification of a Six-Gene Prognostic Signature Characterized by Tumor Microenvironment Immune Profiles in Clear Cell Renal Cell Carcinoma. *Front. Genet.* 12:722421. doi: 10.3389/fgene.2021.722421

Clear cell renal cell carcinoma (ccRCC) is widely acknowledged to be extremely sensitive to immunotherapy, emphasizing the tremendous impacts on which the tumor microenvironment (TME) has shown. However, the molecular subgroups characterized by the TME features scarcely serve as the risk stratification guides in clinical practice for survival outcomes and immunotherapy response prediction. This study generated fresh insights into a novel TME-related prognostic signature derived from The Cancer Genome Atlas database using integrated bioinformatics analyses. Subsequently, Kaplan–Meier survival analysis, receiver operating characteristic analysis, and univariate and multivariate Cox regression analysis were performed to evaluate and validate the efficacy and the accuracy of the signature in ccRCC prognosis. Furthermore, we discovered that the risk score presented an increased likelihood of correlation with miscellaneous clinicopathological characteristics, natural killer cell-mediated cytotoxicity, immune cell infiltration levels, and immune checkpoint expression. These findings highlighted the notion that the six-gene signature characterized by the TME features may have implications on the risk stratification for personalized and precise immunotherapeutic management.

**Keywords:** gene signature, tumor microenvironment, tumor-infiltrating immune cells, immunotherapy, clear cell renal cell carcinoma

## INTRODUCTION

Clear cell renal cell carcinoma (ccRCC) is the most common subtype of renal cancer, making up nearly 70% of the diagnosed individuals (Jonasch et al., 2021; Jonasch et al., 2014; American Cancer Society, 2013). According to the latest guidelines, for patients in the early stage, partial nephrectomy is widely accepted as a preferred approach for a good prognosis (Ljungberg et al., 2015). However, there is no such comfort for patients with metastatic ccRCC, attributing to a striking 11.6% 5-year survival rate compared to 92.5% in patients with early-stage ccRCC (Howlander et al., 2017). Several targeted agents combined with immune checkpoint inhibitors are currently used as the optimal first-line therapy for ccRCC patients (Atkins and Tannir, 2018; Gill et al., 2018; Grimm et al., 2020), which show underestimated effects on distant metastasis control. To date, accumulating studies have shifted their efforts to proposing novel gene signatures or biomarkers that might become the potential tumor-specific targets of ccRCC (Sanchez and Simon, 2018; Ghatalia et al., 2019; Zhang

et al., 2019). However, there are few predictive and robust biomarker guides in the first-line therapy selection practically. The challenge which urgently needs to be taken into account is that the precise risk stratification of patients for selecting the specific treatment strategies remains obscure.

The tumor microenvironment (TME) is a mixture that encompasses a comprehensive set of elements such as tumor cells, immune cells, stromal cells, etc., nourished by the vasculature (Wu and Dai, 2017; Arneith, 2019). Concerning the importance of TME in cancer development and progression, some researchers have proposed their incisive perspectives that the components infiltrating TME consume the crucial nutrients essential for immune surveillance (Delage et al., 2010; Gross et al., 2014; Klysz et al., 2015), which directly undermine the anti-tumor immunity and indirectly proceed tumor progression. Meanwhile, several studies have documented that the TME characteristics may prevent cytotoxicity T lymphocyte (CTL) and natural killer (NK) cells from recognizing and eliminating tumor cells (Cassetta and Kitamura, 2018; Terry et al., 2019; Bonavita et al., 2020), uncovering the underlying mechanism adopted by the TME in tumor immunomodulation. Although many scientists have shed light on identifying the robust biomarkers or gene signatures characterized by TME features that are extensively associated with the aggressive progression of ccRCC (Chevrier et al., 2017; Mier, 2019; Vuong et al., 2019), few risk stratifications based on TME patterns are available in clinical practice.

This study identified robust TME-related biomarkers significantly associated with ccRCC prognosis and constructed a six-gene signature for risk stratification, which discriminates high- and low-risk groups entitled with different prognoses. In addition, this study demonstrated that the prognostic signature might show indispensable implications on modulating the tumor microenvironment and directing immunotherapy intervention in ccRCC.

## METHODS AND MATERIALS

### Data Acquisition From The Cancer Genome Atlas

The gene expression profiles of 525 ccRCC samples were extracted from The Cancer Genome Atlas (TCGA) database (<https://cancergenome.nih.gov>). Samples that met the following criteria were excluded: (1) patients with survival time less than 1 month and (2) patients with incomplete information of TNM, stage, age, gender, and survival time. Then, 468 samples passed the screening and were randomly assigned to the training and validation cohorts by the ratio of 1:1 using random grouping function “sample” in R software. Considering the lack of available and public datasets in clear cell renal cell carcinoma, we hoped to include more samples to validate our findings as much as possible. Therefore, we reset our screening criteria to include the other 51 samples with complete clinical information but with survival time less than 1 month into the validation cohort. As a result, there were 234 samples in the training cohort and 285 samples in the validation cohort. In addition, we included all of the 519 samples into an entire set to further validate our findings.

### Candidate Selection and Gene Signature Construction

The ESTIMATE algorithm could quantify the assessment of the TME characteristics by calculating the immune score, stromal score, and ESTIMATE score (Yoshihara et al., 2013). Only immune score and estimate score passed the preliminary screening, accounting for their high correlations with ccRCC prognosis. A  $p$ -value  $<0.05$  was considered statistically significant in the log-rank test.

The patients were divided into two groups using the mean value of immune score as the cutoff. We did the same grouping analysis according to the ESTIMATE score. With the help of the “limma” package, the differentially expressed genes (DEGs) of the above-mentioned groups that met the criteria of  $p$ -value  $<0.01$  and  $|\log_2 \text{fold change}| >1$  were subjected to Venn analysis, and 240 overlapping DEGs were filtered out. Kaplan–Meier survival analysis was conducted in the training cohort to find the prognostic DEGs. As a result, 149 prognostic DEGs extracted from the intersection of differential expression analysis and survival analysis were imported into the LASSO Cox regression analysis to prevent data overfitting. The LASSO method is a compression estimate applied for the linear models. It could yield a more refined model by compressing some coefficients, while some coefficients are set to zero. As a result, the valuable variables are filtered out, while the unimportant variables are removed. After conducting the LASSO analysis, only six genes were filtered out with their corresponding coefficients. The detected gene signature was constructed after normalization of gene expression, and the risk score equation weighted by LASSO coefficients was as follows:

$$\text{risk score} = \sum_i \text{Coefficient}(mRNA_i) \times \text{Expression}(mRNA_i)$$

### Validation of the Prognostic Signature

The risk score of each patient in the entire cohort was calculated according to the above-mentioned formula. Based on the median score, the patients were divided into high- and low-risk score groups in the training and validation cohorts, respectively. Survival analysis and receiver operating characteristics (ROC) curve analysis (Hanley and McNeil, 1982) were performed to evaluate and validate the prognostic value of the gene signature. In addition, univariate and multivariate Cox regression analyses were used to determine whether the risk score was an independent factor from other clinical parameters in predicting ccRCC clinical outcomes.

### Construction and Validation of Nomogram and Decision Tree

The nomogram is a common method widely used in prognostic models. It could integrate diverse prognostic and determinant parameters to predict the probability of an individual clinical event. In this work, we constructed a nomogram based on the clinical variables and risk score extracted from the univariate and

multivariate Cox regression analyses to predict the overall survival probability of 1, 3, and 5 years. Then, a calibration curve was plotted to visualize the differences between the nomogram and the actual observed outcomes, while the 45° line represents the best predictability. We also constructed a decision tree to further optimize the risk stratification by removing the redundant elements and highlighting the determinants. After all the decisions, each patient was assigned to one of the branches, and then a more refined risk stratification was generated for personalized decisions.

## Functional Analysis and Consensus Clustering Analysis

The Gene Ontology (GO) and Kyoto Encyclopedia of Genes and Genomes (KEGG) enrichment analyses were performed to identify the enriched pathway DEGs between different risk score groups using the “ggplot2” and “GSVA” packages. We downloaded the latest version of the Hallmark (v7.4) and KEGG (v7.4) gene set collections from the Molecular Signatures Database v7.4 download page (<https://www.gsea-msigdb.org/gsea/downloads.jsp>), based on which GSEA analysis was implemented using GSEA software (v4.0.3, <https://www.gsea-msigdb.org/>). Besides this, the Z-score of ssGSEA in the enriched pathway was calculated using the ssGSEA algorithm for normalization (Barbie et al., 2009). According to the optimized  $k$  value, consensus clustering was used to assign the entire samples into different clusters that might share similar characteristics with the R package “ConsensusClusterPlus” based on the six-gene signature expression profiles (Wilkerson and Hayes, 2010). The clusters revealed significantly different molecular characteristics and survival patterns.

## Correlations Between the Risk Score and Immune-Related Features

The 28 immune cell relevant markers were downloaded from the TISIDB database (<http://cis.hku.hk/TISIDB>), a user-friendly web portal integrating comprehensive immune-relevant datasets (Ru et al., 2019). The relative proportions of these tumor-infiltrating immune cells were estimated based on the expression levels of these representative markers with the ssGSEA algorithm. In addition, ESTIMATE algorithm was used to quantify the assessment of TME characteristics to investigate the correlations between the risk scores and TME features. We also compared different distributions of the immune checkpoints in the high-risk and the low-risk groups. The correlation coefficients were calculated and graphically displayed in the lollipop diagram and scatterplots.

## Statistical Analysis

All the statistical calculations and visualizations of the results were conducted with R software, version 4.0.3. The Wilcoxon rank-sum test was used to check for the differences between the two independent groups. The Kaplan–Meier plot was performed to show the survival differences of various stratified analyses, and the statistical differences were examined in the log-rank test.

Pearson analysis was used to verify the significant correlation coefficients in our study. Unless noted particularly,  $p$ -value <0.05 was defined as the statistically significant criteria.

## RESULTS

### Identification of TME-Related DEGs

The present research was simplified to a flow chart as shown in **Supplementary Figure S1**. In order to investigate the correlations of the TME characteristics with clinical features in ccRCC patients, we employed ESTIMATE analysis to calculate the TME score using the “estimate” package for each sample in the training cohort. The median value of the TME scores was defined as the cutoff. Kaplan–Meier survival curves revealed that patients with low immune scores or estimate scores encountered a prolonged survival time compared with the others. However, the stratification analysis based on the stromal score made no statistical significance (**Figures 1A–C**).

Moreover, we observed that the TME scores were closely related to some clinicopathological traits. Apart from the stromal score, immune score, and estimate score, both owned significantly different distributions among various prognosis-related clinical features, such as stage, T classification, and distant metastasis (**Figures 1D–I, Supplementary Figures S2A–C**). In addition, among the three TME scores, only the estimate score was significantly correlated to lymph node metastasis (**Supplementary Figures S2D–F**). Unfortunately, there were no significant differences in status stratification among the three TME scores (**Supplementary Figures S2G–I**). From the perspective of the above-mentioned results, we concluded that immune score and estimate score played a crucial role in ccRCC prognosis, especially in the prediction of survival time and clinicopathological trait discrimination.

### Construction of a Six-Gene-Based Prognostic Signature

Based on the median value of immune score and estimate score as cutoffs, we compared the gene expression profiles between different immune and estimate score groups to further explore the underlying mechanism of TME characteristics involved in ccRCC progression. Differentially expressed genes were defined as those that met the criteria of  $p$ -value <0.01 and  $|\log_2$  fold change| >1 using the R package “limma,” which screened out 479 (**Figures 2A,C**) and 255 DEGs (**Figures 2B,D**) from immune and estimate score groups, respectively. As shown in **Figure 2E**, the Venn diagram displayed 240 overlapping DEGs based on the intersection analysis. Subsequently, Kaplan–Meier analysis was performed to identify 149 common DEGs significantly correlated to overall survival time, which were then imported into LASSO Cox regression analysis in order to prevent overfitting gene signatures (**Figures 2F,G**). We established a novel prognostic gene signature according to the corresponding coefficients calculated by the LASSO algorithm (**Figure 2H**). The risk score formula for each sample was constructed as follows based on the expression levels of these mRNAs: risk score =

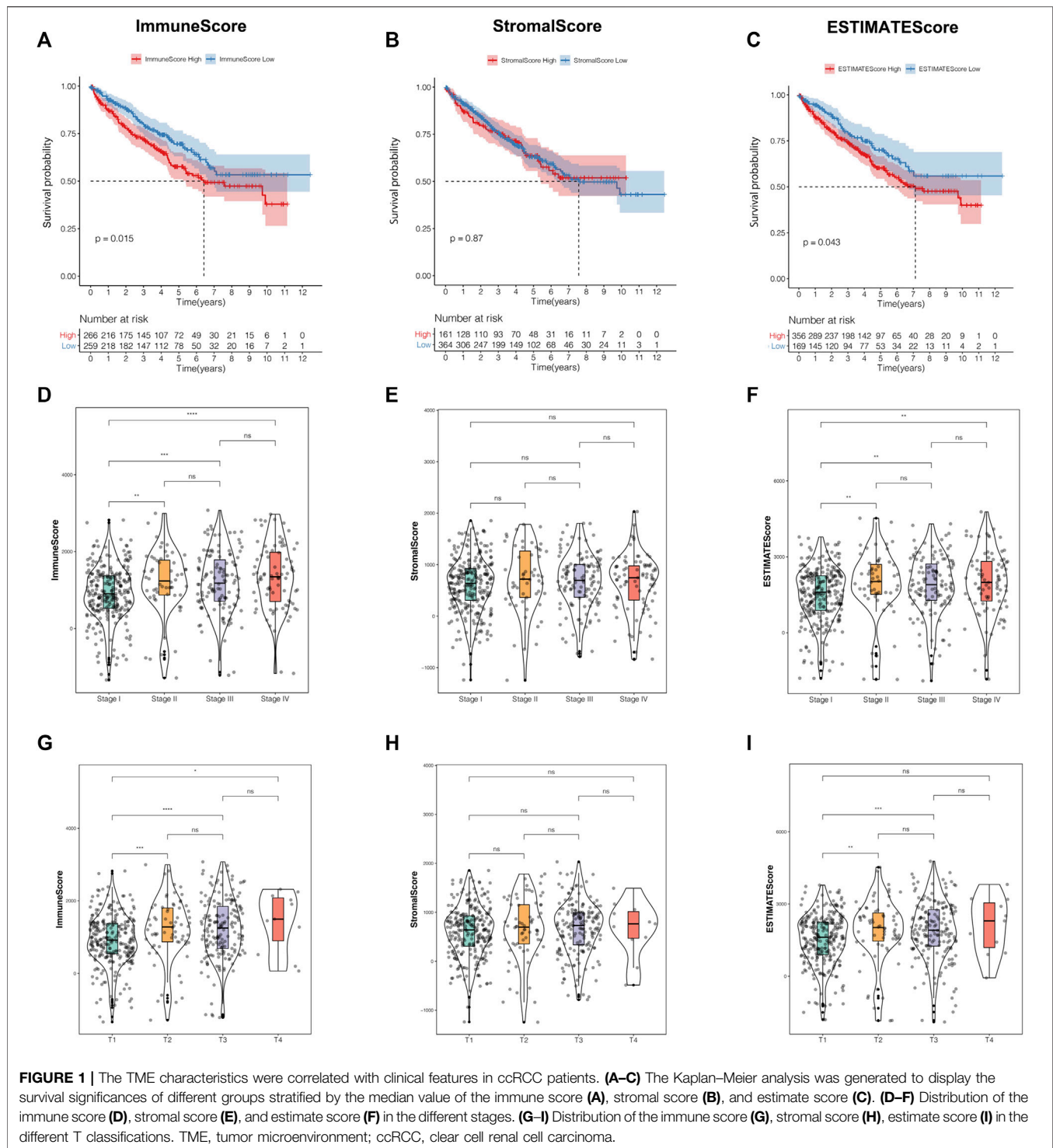
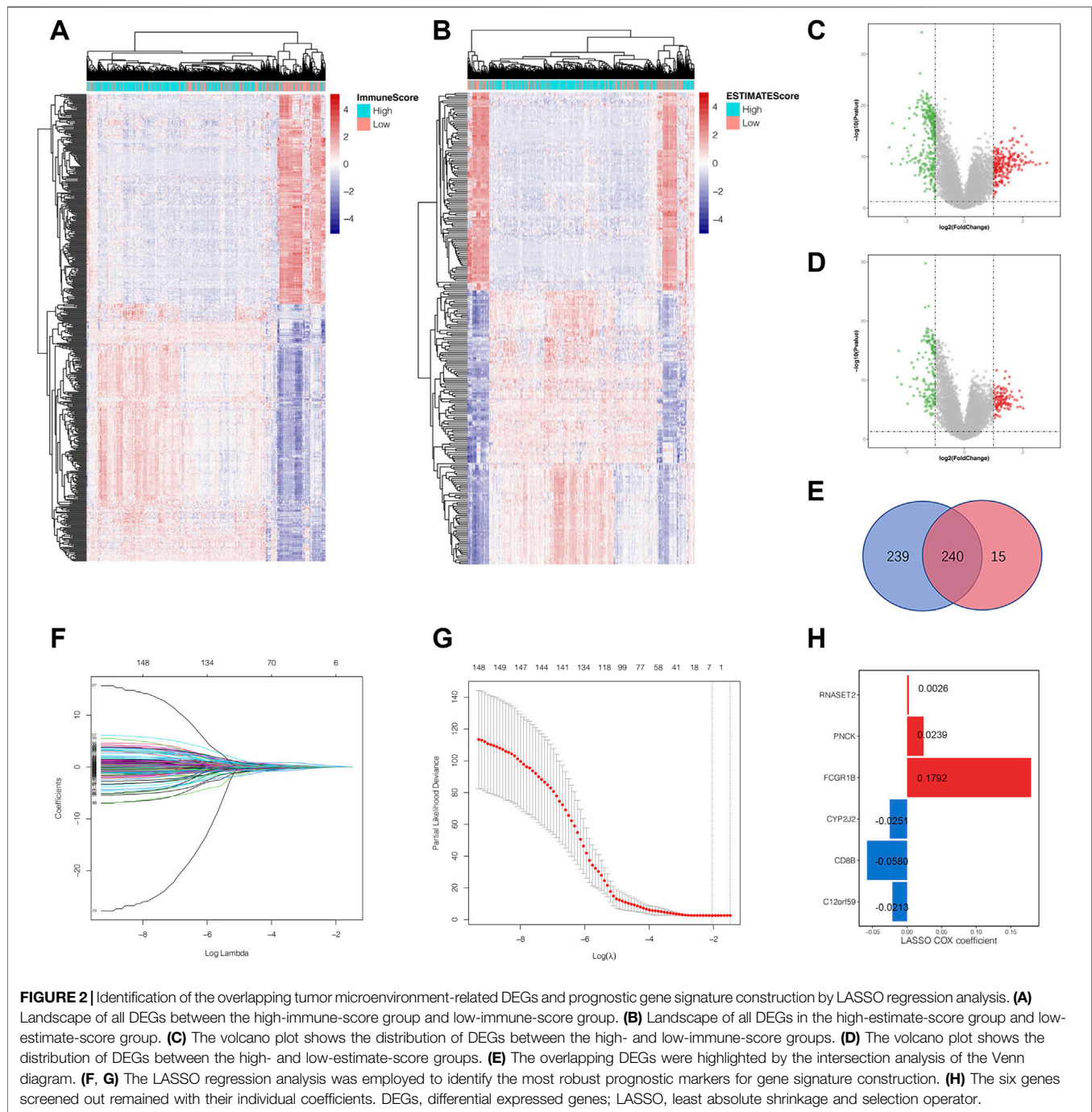


**FIGURE 1 |** The TME characteristics were correlated with clinical features in ccRCC patients. (A–C) The Kaplan–Meier analysis was generated to display the survival significances of different groups stratified by the median value of the immune score (A), stromal score (B), and estimate score (C). (D–F) Distribution of the immune score (D), stromal score (E), and estimate score (F) in the different stages. (G–I) Distribution of the immune score (G), stromal score (H), estimate score (I) in the different T classifications. TME, tumor microenvironment; ccRCC, clear cell renal cell carcinoma.

$RNASET2*0.0026 + PNCK*0.0239 + FCGR1B*0.1792 + CYP2J2*(-0.0251) + CD8B*(-0.0580) + C12orf59*(-0.0213)$ . After a rigorous calculation of gene expression combined with risk coefficients, the ccRCC samples were then divided into the high- and low-risk score groups using the median risk score value as the cutoff.

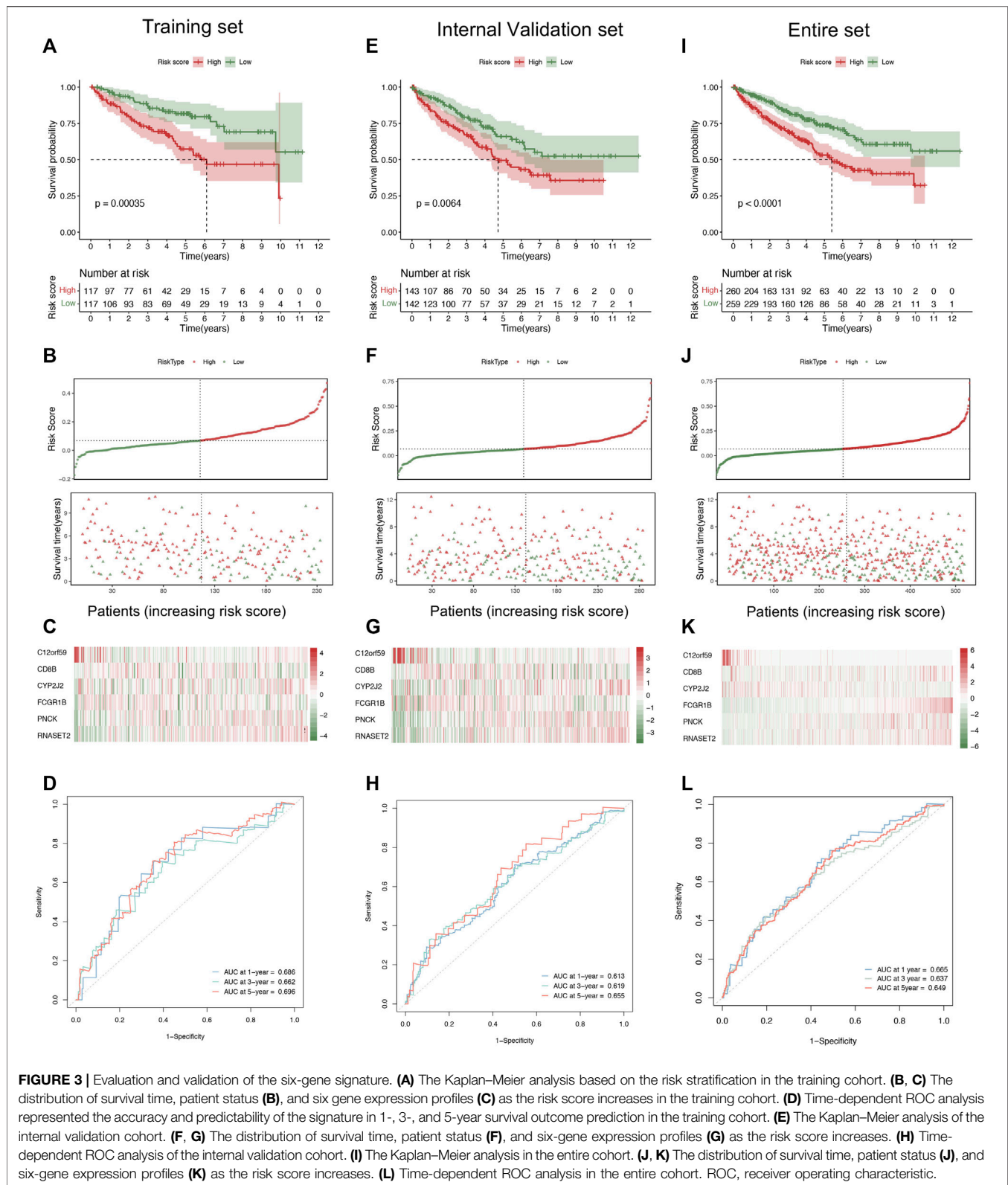
## Evaluation and Validation of Six-Gene Signature

In order to explore the predictive values of the risk score in ccRCC, we conducted several prognosis-related analyses to compare the differences between the high and low groups in the training and validation cohorts, respectively. The



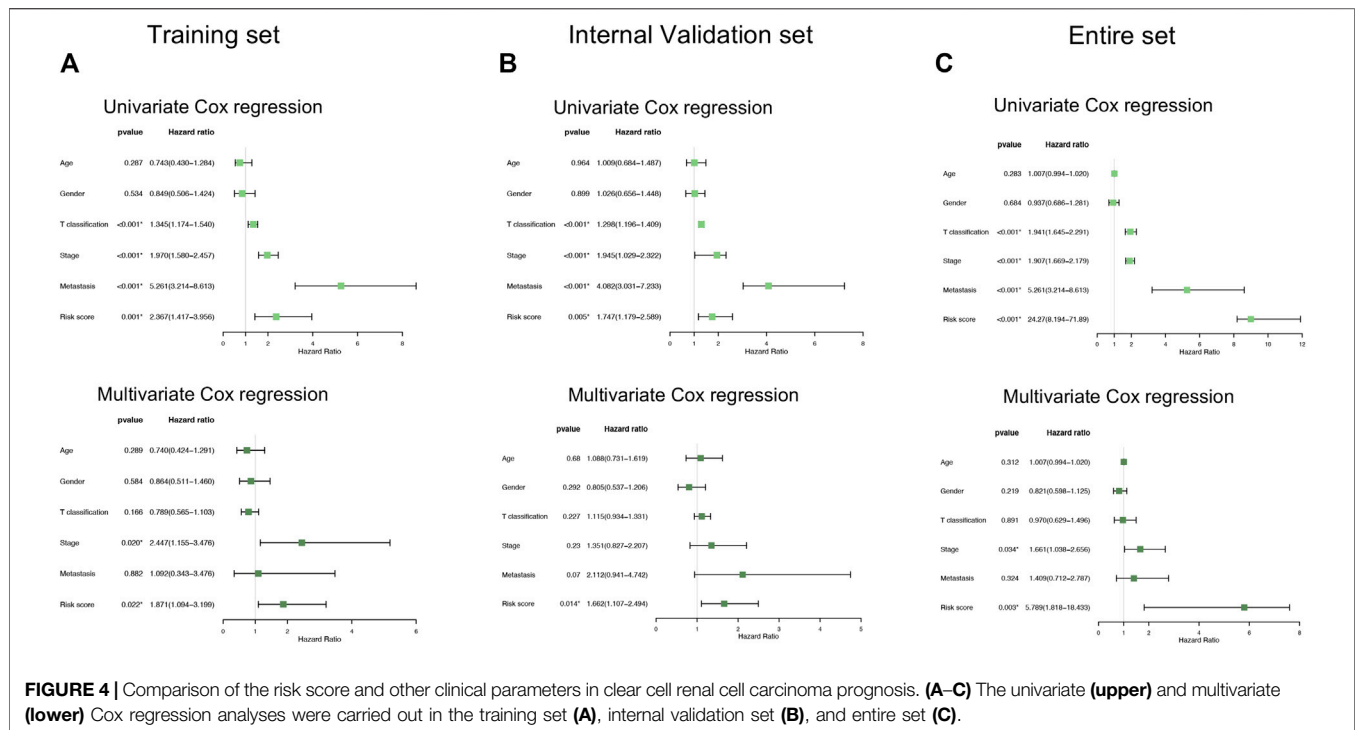
Kaplan–Meier survival analysis indicated that the low-risk score group had a prolonged survival time than the high-risk score group (Figure 3A). Notably, the risk score curve and status scatterplot revealed that the deaths mainly accumulated within the high-risk score area in the training cohort (Figure 3B). As shown in Figure 3C, the heat map showed no significant differences between risk scores and the six gene expression profiles, attributing to the limited quantities of the samples. Moreover, time-dependent ROC curves indicated that the area under the ROC curve (AUC) values of 1-, 3-,

and 5-year survival were all above 0.65 (Figure 3D), which demonstrated the predictability and the accuracy of the six-gene signature in ccRCC prognosis. To further validate the predictive efficacy of the signature, we conducted the same prognosis-related analyses in the internal validation cohort (Figures 3E–H) and the entire cohort (Figure 3I–L), which turned out to strikingly resemble those in the training cohort. Therefore, we concluded that the six-gene pattern correlated highly to ccRCC prognosis, exhibiting the excellent potential in predicting survival outcomes. As a



result, the high-risk score conferred relatively poor clinical outcomes, while the low-risk score conferred a prolonged survival time.

We also conducted univariate and multivariate Cox regression analyses in the training and validation cohorts, which focused on several clinicopathological parameters, such as age, gender, T



classification, stage, and distant metastasis as well as risk score (Figures 4A–C). From the perspectives of the intersection results, we observed that the risk score stratification might hopefully become a potential and independent factor beyond the other variables concerning the capacity of the prediction in overall survival time.

## The Six-Gene Signature Correlated With the Clinicopathological Traits of ccRCC Patients

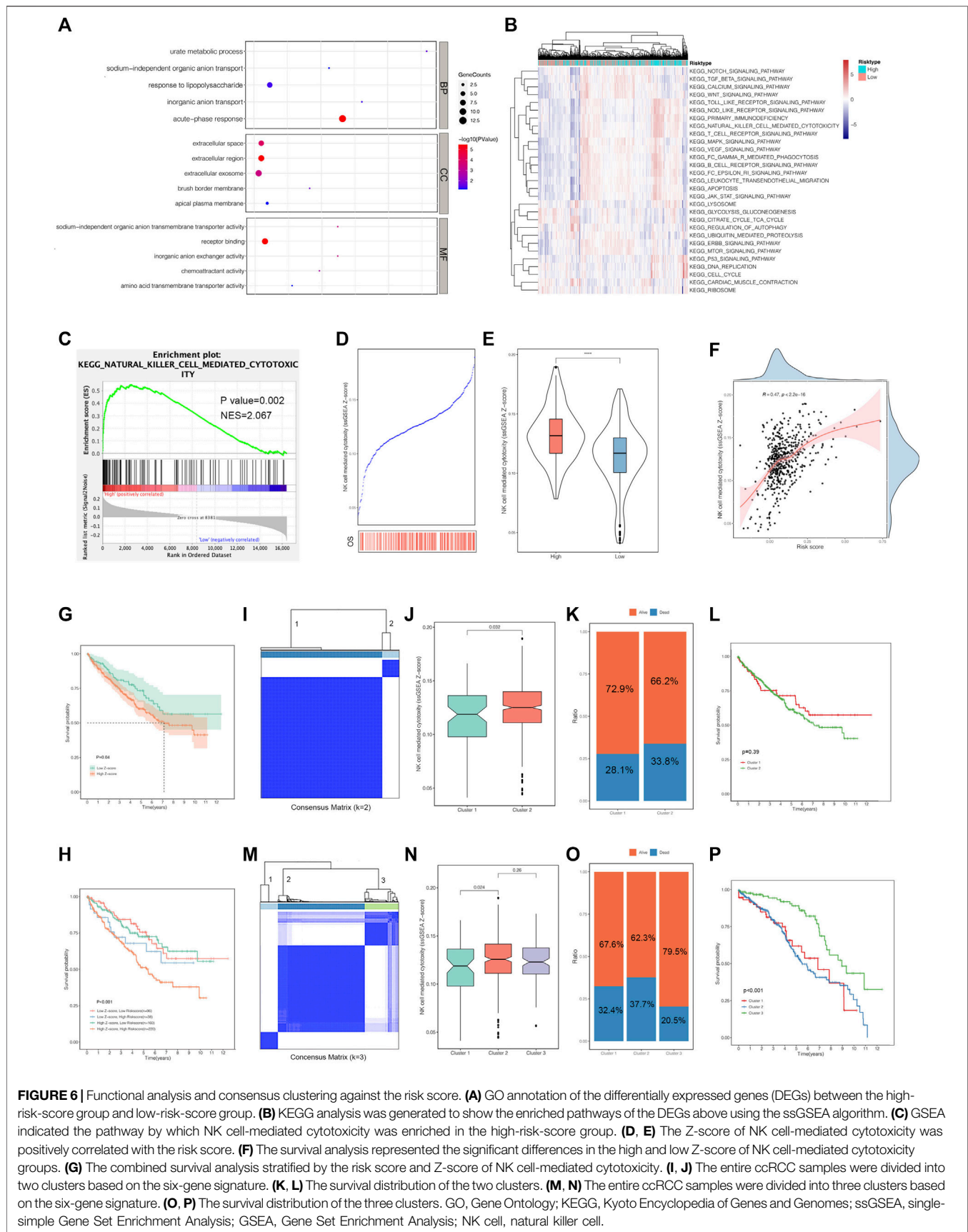
The correlations between the six-gene signature and clinical characteristics were further explored in the entire cohorts. The results supported that status, gender, metastasis, stage, and T classification were significantly correlated with the risk scores, while age was not (Figures 5A–F). The high-risk scores indicated more deaths, males, and distant metastasis diseases. In addition, patients divided into later stages and T classification tended to manifest high-risk scores. Subsequently, all the patients were separated into several groups according to clinicopathological features. The Kaplan–Meier survival curves of these groups revealed that the risk stratification represented a good prediction ability in ccRCC prognosis among diverse subgroups. Consistently, the patients with low-risk scores had a better prognosis than those with high scores in female ( $p = 0.014$ ), male ( $p < 0.001$ ), M0 ( $p = 0.01$ ), M1 ( $p = 0.0088$ ), stage III ( $p < 0.019$ ), stage IV ( $p = 0.027$ ), and T4 ( $p < 0.001$ ) subgroups (Figures 5G–J).

## Functional Enrichment and Consensus Clustering Analysis With the Risk Scores

Considering the positive correlations between the risk scores and multiple clinical features, we performed GO functional annotation and KEGG enrichment analyses based on the ssGSEA algorithm to quantify the enriched pathway levels of DEGs between high- and low-risk score groups. In view of the results, we observed that acute-phase response was enriched in the biological process term, while extracellular space, extracellular region, and extracellular exosome were in the cellular component term. For molecular function (MF) term, receptor binding was significantly involved (Figure 6A). In addition, the KEGG analysis supported that risk score was positively correlated with immune-related pathways, such as NK cell-mediated cytotoxicity, T cell receptor signaling pathway, leukocyte trans-endothelial migration, *etc.* (Figure 6B).

In order to get deep insights into the correlations between risk score and immune-related pathway, we also conducted GSEA analysis based on the risk stratification, which tended to be mutually consistent as previously illustrated. NK cell-mediated cytotoxicity owned significances beyond others (Figure 6C). Subsequently, a comparison of NK cell-mediated cytotoxicity and risk score was established to determine whether the combination could optimize the original model in ccRCC prognosis. The results suggested that the Z-scores of NK cell-mediated cytotoxicity gained in the ssGSEA algorithm were obviously higher in deaths than those alive during follow-up (Figure 6D). Besides this, we confirmed that the Z-scores of the





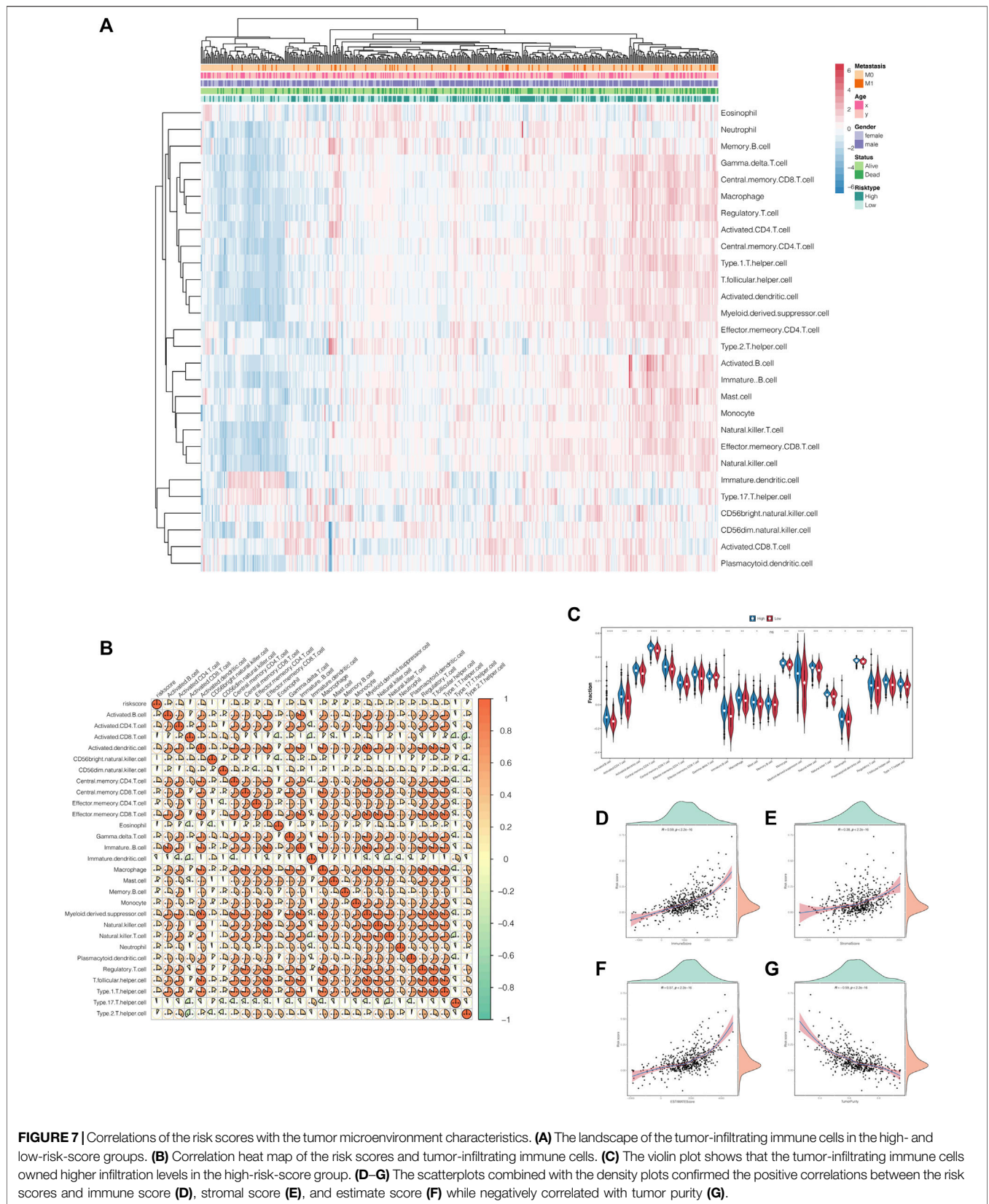
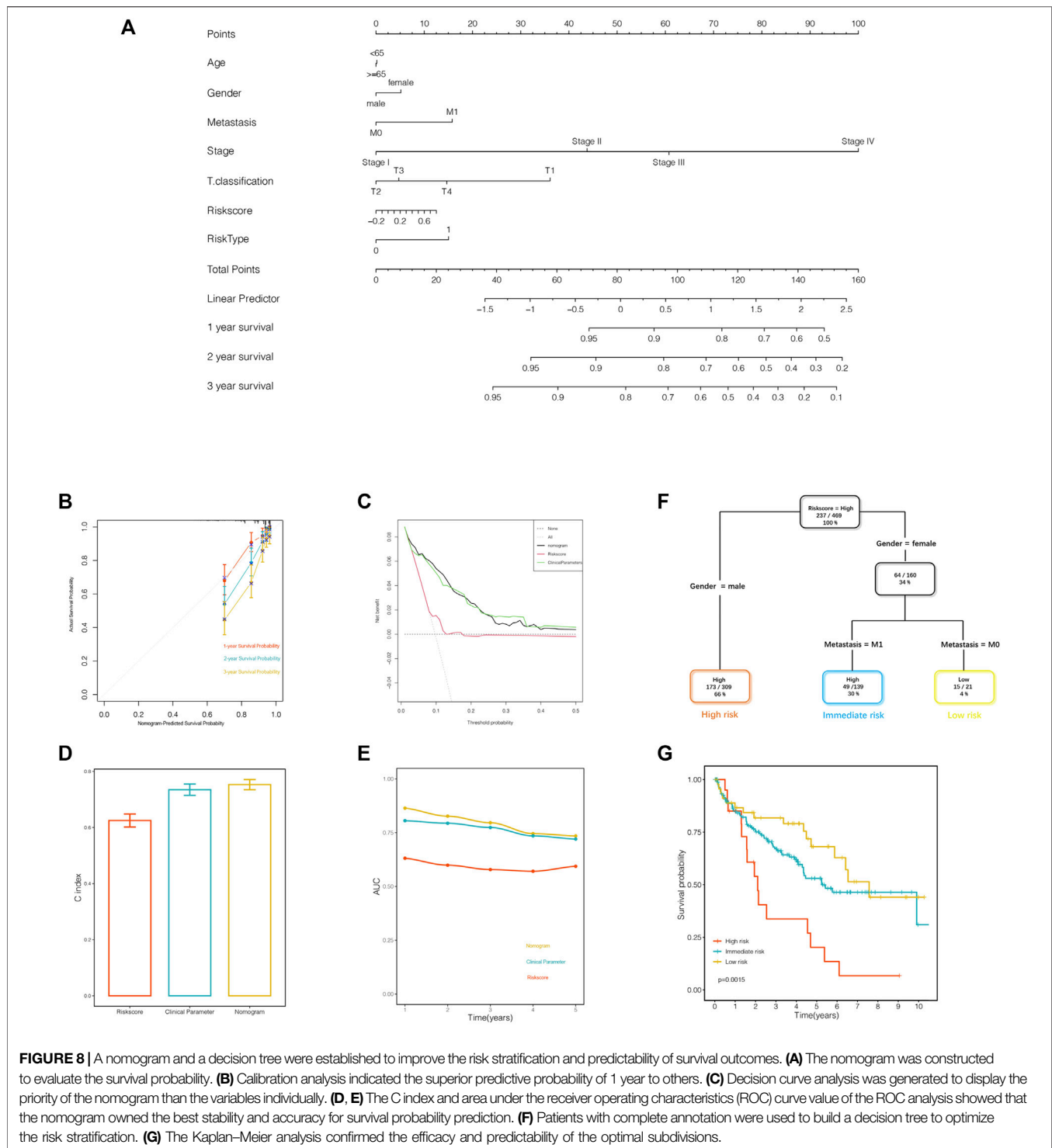


**FIGURE 7 |** Correlations of the risk scores with the tumor microenvironment characteristics. **(A)** The landscape of the tumor-infiltrating immune cells in the high- and low-risk-score groups. **(B)** Correlation heat map of the risk scores and tumor-infiltrating immune cells. **(C)** The violin plot shows that the tumor-infiltrating immune cells owned higher infiltration levels in the high-risk-score group. **(D–G)** The scatterplots combined with the density plots confirmed the positive correlations between the risk scores and immune score **(D)**, stromal score **(E)**, and estimate score **(F)** while negatively correlated with tumor purity **(G)**.



NK cell-mediated cytotoxicity was positively corresponding to the risk scores (Figures 6E,F), inspiring us to perform the survival analysis based on the stratification of the above-mentioned Z-scores. As expected, the high Z-score ones encountered a shorter survival time than the low ones with  $p$ -value of 0.04 (Figure 6G). In addition, a survival analysis combined with the above-mentioned two components was performed to clarify the

intricate relationships among them. The results revealed that the patients with low Z-scores and low-risk scores had a prolonged survival compared to those with low Z-scores and high-risk scores, and patients with high-risk scores were associated with a poorer prognosis than those with low-risk scores based on the same high-Z-score subgroups (Figure 6H). Generally, the risk score could reflect the Z-scores of the NK cell-mediated

cytotoxicity. The combined model of the above-mentioned two variables might optimize the original risk stratification for ccRCC prognosis.

Consensus clustering analysis divided the entire samples into different clusters according to the optimal  $k$  value based on the six-gene signature expression pattern (Figure 6I,M, Supplementary Figure S3). When the  $k$  value was 2, we observed the particular significances of Z-scores of the NK cell-mediated cytotoxicity and the status distribution between the two clusters (Figures 6J,K). However, as shown in Figure 6L, the survival analysis did not exhibit significant differences. Differently from what was previously explained, when the  $k$  value was 3, the Z-scores of the NK cell-mediated cytotoxicity of the patients in cluster 1 was significantly different from those in cluster 2 (Figure 6N). The distinct distribution of status stratified by these three clusters is displayed in Figure 6O, and we observed that patients involved in cluster 3 had a superior prognosis to the others (Figure 6P). Given the above-mentioned results, we deduced that the  $k$  value of 3 manifested pronounced performances in risk stratification beyond the  $k$  value of 2.

## Correlations of Risk Scores With the Proportion of Tumor-Infiltrating Immune Cells and Immune Checkpoints

As previously explained, risk scores did correlate with immune-related pathways. Therefore, to further investigate the latent impacts risk scores had on immunity, we extended the ssGSEA algorithm to estimate the proportion of tumor-infiltrating immune cells in ccRCC patients. As shown in Figure 7A, the heat maps represented the landscape wherein most of the immune cells gained higher ssGSEA scores in the high-risk score group, which meant that risk score was positively correlated to immunity activation (Figure 7B). Moreover, the violin plots graphically displayed that high-risk score conferred high immune cell infiltration levels (Figure 7C). We also portrayed the correlations between risk scores and TME characteristics in scatterplots combined with density plots. The results demonstrated that stromal score, immune score, and estimate score were highly and positively associated with risk score, while tumor purity was negatively associated with it (Figures 7D–G).

Interestingly, we compared the expression of immune checkpoints between the high- and low-risk score groups and concluded that the risk stratification might play a crucial role as an indicator of immune checkpoint efficacy, accounting for the positive and significant correlations among them (Supplementary Figure S4).

## Combination of the Gene Signature and Clinical Parameters Improved Risk Stratification and Survival Outcome Prediction

The nomogram was established to quantify the survival probability of an individual clinical event with a risk score, along with other clinical parameters as illustrated previously

(Figure 8A). In order to evaluate the efficacy of the nomogram in survival time prediction, we conducted several validation analyses from four distinct perspectives. The prediction line of the 1-year survival ability was practically coincident with the ideal performance compared to 2- or 3-year survival ability in the calibration analysis (Figure 8B), indicating the accuracy of the nomogram in the early period for practical application. As displayed in Figure 8C, the decision curve analysis corroborated that the nomogram, as well as the clinical parameters, obtained much more net benefit of survival probability than the risk score alone. In addition, the C index and AUC value synergistically confirmed that the nomogram provided a superior prognostic value beyond the other variables (Figures 8D,E).

The entire samples with informative clinical annotation and risk score assessment were subjected to establish a decision tree in order to optimize the risk subdivision of overall survival. As shown in Figure 8F, only risk score, gender, and distant metastasis were still retained in the decision tree, and three subgroups were defined according to the above-mentioned three parameters. In the optimized stratification, gender was identified as the cutoff in the high-risk score branch, while distant metastasis replaced gender in the female branch. Interestingly, the survival analysis showed significant differences based on the latest risk subdivision, which was consistent with the survival time prediction (Figure 8G). In summary, both the nomogram system and the decision tree obtained remarkable achievements in optimizing risk stratification and survival outcome prediction, attributing to taking risk score synergistically with clinical parameters into consideration.

## DISCUSSION

To our best knowledge, few studies commit to adopting the risk discrimination of ccRCC related to TME characteristics as a direction in clinical practice, which is exactly the blank our study spares no pain to fill. Based on the high-throughput data and clinical information obtained from the TCGA database, we established a six-gene prognostic signature of pronounced correlations with the TME characteristics with the help of integrated statistical methods. In the training cohort, Kaplan–Meier survival analysis, ROC analysis, and univariate and multivariate Cox analyses were performed to evaluate the predictive capability of the signature in ccRCC prognosis. Subsequently, the dominant findings were confirmed to be repeatable in the validation cohorts using the same statistical methods. In addition, we observed that the signature was distinctly correlated to the infiltration levels of tumor-infiltrating cells and immune checkpoint expression, indicating that the risk stratification might serve as a novel criterion of the management of immunotherapy and patient selection.

After the construction of the prognostic signature, we evaluated the predictability of clinical outcomes based on the stratification of risk scores. We observed that the high-risk zone owned more deaths as well as a shorter survival time. These

findings were reproducible in the validation cohorts. Given the above-mentioned results, we concluded that the risk score was negatively correlated to ccRCC prognosis. In addition, the time-dependent ROC analysis confirmed the accuracy and predictability of the signature in long-term prognosis. The univariate and multivariate Cox analysis suggested that the risk score was a pronounced and independent factor of predicting ccRCC outcomes. The corresponding ROC analysis confirmed that the risk score was superior to other clinical parameters. To further investigate the relationships between the risk score and clinical characteristics, we extended the risk score distribution and survival analysis based on different groups stratified by clinical characteristics. The results turned out that the high-risk scores gave rise to more deaths, high-level of clinical-pathological features, and shorter survival time, further verified the findings as previously illustrated.

In order to explore the underlying mechanism that the signature adopted to modulate cancer development and progression, we performed functional analysis to compare the enriched pathways of DEGs derived from high- and low-risk score groups and observed that immune-related and carcinogenetic pathways stand out due to their pronounced performances. Natural killer (NK) cell is generally acknowledged to commit to induce immunosurveillance and hamper tumor aggressive progression through apoptosis activation (Yang et al., 2017; Prager and Watzl, 2019; Sordo-Bahamonde et al., 2020). A previous study agreed that a combined strategy of re-active NK cells and other conventional therapies might give rise to an ideal curative effect for lung cancer patients (Pockley et al., 2020). In the past few decades, several immune-targeted agents for breast cancer that trigger NK cell mediated cytotoxicity have been tested in clinical trials or cell lines (Collins et al., 2012; Juliá et al., 2018). Therefore, we constructed correlation analysis, and survival analysis against NK cell mediated cytotoxicity and observed that it was positively correlated with the risk score. The high Z-score of NK cell mediated cytotoxicity conferred to poor prognosis. Besides, the combination survival analysis of risk score and NK cell mediated cytotoxicity revealed that patients with low levels of these two characters encountered the shortest survival time compared to the others. Taking these findings into account, we supposed that patients assigned to high-risk score groups synergistically with high Z-scores might show greater response on the corresponding NK cell-targeted agents, indicating a novel immunotherapy prospect of ccRCC. Based on the widespread of consensus clustering used in genetic researches recently (Cancer Genome Atlas Resea, 2011; Cancer Genome Atlas Resea, 2012; Cancer Genome Atlas Research Network et al., 2013), we also conducted consensus clustering analysis to optimize the subdivisions for better class discovery (Monti et al., 2003), whose efficacy in prognosis prediction was substantiated in the follow-up survival analysis. Liu et al. considered that tumor-infiltrating immune cells play crucial roles in clinical outcomes prediction and immunotherapy efficacy of lung cancer (Liu et al., 2017). According to another study, kidney cancer expressing high levels

of TIM3 separate into two groups in regard to CD8 T-cell infiltration, which may show different implications on immunotherapy targeted TIM3 (Li et al., 2016). The last decades have witnessed great advances taken in tumor-targeted therapy, especially targeting dendritic cells (DCs), known as the dominants in the TME that hinder tumor progression (Banchereau and Steinman, 1998; Steinman and Banchereau, 2007; Tran Janco et al., 2015). The correlation analysis in our study revealed that high-risk score conferred to high levels of the majority of tumor-infiltrating immune cells, indicating that high-risk score groups might exhibit activated immune cells-targeted therapy response. Several studies have demonstrated that tumors exhausted DCs through inducing PD-1 expression in order for immune evasion, which can be reversed unless blockade of PD-1 (Krempski et al., 2011; Karyampudi et al., 2014; Dammeijer et al., 2020). In addition, the mechanism that the interaction of tumor-infiltrating lymphocytes expressing PD-1 and PD-L1 undermine antitumor immunity is generally adopted by cancer immunotherapy (Wang et al., 2014; Kurozumi et al., 2017). Tu et al. observed that PD-1 expression was significantly related to several immune cells in many malignancies (Tu et al., 2020). Considering the positively pairwise correlations between tumor-infiltrating immune cells and risk score, PD-1 expression and tumor-infiltrating immune cells, it was reasonable to assume that risk score might share unknown correlations with PD-1. Therefore, the corresponding results supported that many common immune checkpoints gained high expression levels in the high-risk score group, as well as the positive correlation coefficients against the risk score. In the view of the above, we concluded that this risk stratification owned the potential to broaden a new landscape of evaluating immune checkpoint inhibitors response and implementing immunotherapy intervention. Benefited from the nomogram and decision tree, the current six-gene signature was optimized and merged with clinical parameters in order to improve the predictability of ccRCC outcomes. The assessment from four different aspects confirmed the superiority of the combined model compared with the original signature and clinical parameters alone (Xiong et al., 2018; Wang et al., 2020). Besides this, the decision tree made the subdivision based on the specific clinical parameters, which separated the entire cohorts into three subgroups: high-risk group, median-risk group, and low-risk group (Sun et al., 2020; Shi et al., 2021). The subsequent survival analysis revealed the significant differences among the three subgroups, substantiating the necessity of the improved risk stratification.

Generally, in this study, we constructed a six-gene signature, comprehensively evaluated its prognostic values, and correlated this signature with TME-related characteristics among 519 ccRCC samples using an ensemble of integrated analyses. The dominant findings lay the important foundation for optimizing the risk stratification in ccRCC prognosis and understanding the complex intersection relationships with TME modulation. Hopefully, this signature might broaden our cognitions of TME characteristics entitled with tumor progression and propose a new direction in immunotherapy surveillance. Pertaining to the limited data obtained

from the TCGA database, these findings need to be further corroborated in a larger cohort or in cytological experiments.

## DATA AVAILABILITY STATEMENT

The original contributions presented in the study are included in the article/**Supplementary Material**. Further inquiries can be directed to the corresponding author.

## AUTHOR CONTRIBUTIONS

LZ and MZ contributed to the conceptualization. LW, TY, and QS contributed to the methodology. LZ took charge of the software. Validation was conducted by XL, MM, and NZ. Investigation was carried out by LZ, MJ, and RS. LZ and JL

contributed to writing—original draft preparation. JF contributed to writing—review and editing. All authors have read and agreed to the published version of the manuscript.

## ACKNOWLEDGMENTS

We would like to sincerely appreciate all colleagues from the Department of Urology, The First Affiliated Hospital of Xi'an Jiaotong University, for their support.

## SUPPLEMENTARY MATERIAL

The supplementary material for this article can be found online at: <https://www.frontiersin.org/articles/10.3389/fgene.2021.722421/full#supplementary-material>

## REFERENCES

- American Cancer Society (2013). *Cancer Facts & Figures*.
- Arneth, B. (2019). Tumor Microenvironment. *Medicina (Kaunas)* 56 (1), 15. doi:10.3390/medicina56010015
- Atkins, M. B., and Tannir, N. M. (2018). Current and Emerging Therapies for First-Line Treatment of Metastatic clear Cell Renal Cell Carcinoma. *Cancer Treat. Rev.* 70, 127–137. doi:10.1016/j.ctrv.2018.07.009
- Banchereau, J., and Steinman, R. M. (1998). Dendritic Cells and the Control of Immunity. *Nature* 392, 245–252. doi:10.1038/32588
- Barbie, D. A., Tamayo, P., Boehm, J. S., Kim, S. Y., Moody, S. E., Dunn, I. F., et al. (2009). Systematic RNA Interference Reveals that Oncogenic KRAS-Driven Cancers Require TBK1. *Nature* 462 (7269), 108–112. doi:10.1038/nature08460
- Bonavita, E., Bromley, C. P., Jonsson, G., Pelly, V. S., Sahoo, S., Walwyn-Brown, K., et al. (2020). Antagonistic Inflammatory Phenotypes Dictate Tumor Fate and Response to Immune Checkpoint Blockade. *Immunity* 53 (6), 1215–1229.e8. doi:10.1016/j.immuni.2020.10.020
- Cancer Genome Atlas Research Network (2012). Comprehensive Molecular Portraits of Human Breast Tumours. *Nature* 490, 61–70. doi:10.1038/nature11412
- Cancer Genome Atlas Research Network (2011). Integrated Genomic Analyses of Ovarian Carcinoma. *Nature* 474, 609–615. doi:10.1038/nature10166
- Cancer Genome Atlas Research NetworkKandath, C., Schultz, N., Cherniack, A. D., Akbani, R., Liu, Y., Shen, H., et al. (2013). Integrated Genomic Characterization of Endometrial Carcinoma. *Nature* 497, 67–73. doi:10.1038/nature12113
- Cassetta, L., and Kitamura, T. (2018). Macrophage Targeting: Opening New Possibilities for Cancer Immunotherapy. *Immunology* 155 (3), 285–293. doi:10.1111/imm.12976
- Chevrier, S., Levine, J. H., Zanotelli, V. R. T., Silina, K., Schulz, D., Bacac, M., et al. (2017). An Immune Atlas of Clear Cell Renal Cell Carcinoma. *Cell* 169 (4), 736–749.e18. doi:10.1016/j.cell.2017.04.016
- Collins, D. M., O'Donovan, N., McGowan, P. M., O'Sullivan, F., Duffy, M. J., and Crown, J. (2012). Trastuzumab Induces Antibody-dependent Cell-Mediated Cytotoxicity (ADCC) in HER-2-Non-Amplified Breast Cancer Cell Lines. *Ann. Oncol.* 23 (7), 1788–1795. doi:10.1093/annonc/mdr484
- Dammeijer, F., van Gulijk, M., Mulder, E. E., Lukkes, M., Klaase, L., van den Bosch, T., et al. (2020). The PD-1/pd-L1-Checkpoint Restrains T Cell Immunity in Tumor-Draining Lymph Nodes. *Cancer Cell* 38 (5), 685–700.e8. doi:10.1016/j.ccell.2020.09.001
- Delage, B., Fennell, D. A., Nicholson, L., McNeish, I., Lemoine, N. R., Crook, T., et al. (2010). Arginine Deprivation and Argininosuccinate Synthetase Expression in the Treatment of Cancer. *Int. J. Cancer* 126, 2762–2772. doi:10.1002/ijc.25202
- Ghatalia, P., Gordetsky, J., Kuo, F., Dulaimi, E., Cai, K. Q., Devarajan, K., et al. (2019). Prognostic Impact of Immune Gene Expression Signature and Tumor Infiltrating Immune Cells in Localized clear Cell Renal Cell Carcinoma. *J. Immunother. Cancer* 7 (1), 139. doi:10.1186/s40425-019-0621-1
- Gill, D. M., Hahn, A. W., Hale, P., and Maughan, B. L. (2018). Overview of Current and Future First-Line Systemic Therapy for Metastatic Clear Cell Renal Cell Carcinoma. *Curr. Treat. Options. Oncol.* 19 (1), 6. doi:10.1007/s11864-018-0517-1
- Grimm, M. O., Leucht, K., Grünwald, V., and Foller, S. (2020). New First Line Treatment Options of Clear Cell Renal Cell Cancer Patients with PD-1 or PD-L1 Immune-Checkpoint Inhibitor-Based Combination Therapies. *J. Clin. Med.* 9 (2), 565. doi:10.3390/jcm9020565
- Gross, M. I., Demo, S. D., Dennison, J. B., Chen, L., Chernov-Rogan, T., Goyal, B., et al. (2014). Antitumor Activity of the Glutaminase Inhibitor CB-839 in Triple Negative Breast Cancer. *Mol. Cancer Ther.* 13, 890–901. doi:10.1158/1535-7163.mct-13-0870
- Hanley, J. A., and McNeil, B. J. (1982). The Meaning and Use of the Area under a Receiver Operating Characteristic (ROC) Curve. *Radiology* 143, 29–36. doi:10.1148/radiology.143.1.7063747
- Howlander, N., Noone, A. M., Krapcho, M., Miller, D., Bishop, K., Kosary, C. L., Cronin, K. A., et al. (2017). *SEER Cancer Statistics Review, 1975-2014, Based on November 2016 SEER Data Submission, Posted to the SEER Web Site*. Bethesda, MD: National Cancer Institute.
- Jonasch, E., Gao, J., and Rathmell, W. K. (2014). Renal Cell Carcinoma. *BMJ* 349, g4797. doi:10.1136/bmj.g4797
- Jonasch, E., Walker, C. L., and Rathmell, W. K. (2021). Clear Cell Renal Cell Carcinoma Ontogeny and Mechanisms of Lethality. *Nat. Rev. Nephrol.* 17 (4), 245–261. doi:10.1038/s41581-020-00359-2
- Juliá, E. P., Amante, A., Pampena, M. B., Mordoh, J., and Levy, E. M. (2018). Avelumab, an IgG1 Anti-PD-L1 Immune Checkpoint Inhibitor, Triggers NK Cell-Mediated Cytotoxicity and Cytokine Production against Triple Negative Breast Cancer Cells. *Front. Immunol.* 9, 2140. doi:10.3389/fimmu.2018.02140
- Karyampudi, L., Lamichhane, P., Scheid, A. D., Kalli, K. R., Shreeder, B., Krempski, J. W., et al. (2014). Accumulation of Memory Precursor CD8 T Cells in Regressing Tumors Following Combination Therapy with Vaccine and Anti-PD-1 Antibody. *Cancer Res.* 74, 2974. doi:10.1158/0008-5472.can-13-2564
- Klysz, D., Tai, X., Robert, P. A., Craveiro, M., Cretenet, G., Oburoglu, L., et al. (2015). Glutamine-dependent  $\alpha$ -ketoglutarate Production Regulates the Balance between T Helper 1 Cell and Regulatory T Cell Generation. *Sci. Signal.* 8 (396), ra97. doi:10.1126/scisignal.aab2610
- Krempski, J., Karyampudi, L., Behrens, M. D., Erskine, C. L., Hartmann, L., Dong, H., et al. (2011). Tumor-infiltrating Programmed Death Receptor-1+ Dendritic Cells Mediate Immune Suppression in Ovarian Cancer. *J. Immunol.* 186, 6905–6913. doi:10.4049/jimmunol.1100274

- Kurozumi, S., Fujii, T., Matsumoto, H., Inoue, K., Kurozumi, M., Horiguchi, J., et al. (2017). Significance of Evaluating Tumor-Infiltrating Lymphocytes (TILs) and Programmed Cell Death-Ligand 1 (PD-L1) Expression in Breast Cancer. *Med. Mol. Morphol.* 50 (4), 185–194. doi:10.1007/s00795-017-0170-y
- Li, B., Severson, E., Pignon, J. C., Zhao, H., Li, T., Novak, J., et al. (2016). Comprehensive Analyses of Tumor Immunity: Implications for Cancer Immunotherapy. *Genome Biol.* 17 (1), 174. doi:10.1186/s13059-016-1028-7
- Liu, X., Wu, S., Yang, Y., Zhao, M., Zhu, G., and Hou, Z. (2017). The Prognostic Landscape of Tumor-Infiltrating Immune Cell and Immunomodulators in Lung Cancer. *Biomed. Pharmacother.* 95, 55–61. doi:10.1016/j.biopha.2017.08.003
- Ljungberg, B., Bensalah, K., Canfield, S., Dabestani, S., Hofmann, F., Hora, M., et al. (2015). EAU Guidelines on Renal Cell Carcinoma: 2014 Update. *Eur. Urol.* 67 (5), 913–924. doi:10.1016/j.eururo.2015.01.005
- Mier, J. W. (2019). The Tumor Microenvironment in Renal Cell Cancer. *Curr. Opin. Oncol.* 31 (3), 194–199. doi:10.1097/cco.0000000000000512
- Monti, S., Tamayo, P., Mesirov, J., and Golub, T. (2003). Consensus Clustering: A Resampling-Based Method for Class Discovery and Visualization of Gene Expression Microarray Data. *Machine Learn.* 52, 91–118. doi:10.1023/a:1023949509487
- Pockley, A. G., Vaupel, P., and Multhoff, G. (2020). NK Cell-Based Therapeutics for Lung Cancer. *Expert Opin. Biol. Ther.* 20 (1), 23–33. doi:10.1080/14712598.2020.1688298
- Prager, I., and Watzl, C. (2019). Mechanisms of Natural Killer Cell-Mediated Cellular Cytotoxicity. *J. Leukoc. Biol.* 105 (6), 1319–1329. doi:10.1002/jlb.mr0718-269r
- Ru, B., Wong, C. N., Tong, Y., Zhong, J. Y., Zhong, S. S. W., Wu, W. C., et al. (2019). TISIDB: an Integrated Repository portal for Tumor-Immune System Interactions. *Bioinformatics* 35 (20), 4200–4202. doi:10.1093/bioinformatics/btz210
- Sanchez, D. J., and Simon, M. C. (2018). Genetic and Metabolic Hallmarks of clear Cell Renal Cell Carcinoma. *Biochim. Biophys. Acta Rev. Cancer* 1870 (1), 23–31. doi:10.1016/j.bbcan.2018.06.003
- Shi, R., Bao, X., Unger, K., Sun, J., Lu, S., Manapov, F., et al. (2021). Identification and Validation of Hypoxia-Derived Gene Signatures to Predict Clinical Outcomes and Therapeutic Responses in Stage I Lung Adenocarcinoma Patients. *Theranostics* 11 (10), 5061–5076. doi:10.7150/thno.56202
- Sordo-Bahamonde, C., Lorenzo-Herrero, S., Payer, Á. R., Gonzalez, S., and López-Soto, A. (2020). Mechanisms of Apoptosis Resistance to NK Cell-Mediated Cytotoxicity in Cancer. *Int. J. Mol. Sci.* 21 (10), 3726. doi:10.3390/ijms21103726
- Steinman, R. M., and Banchereau, J. (2007). Taking Dendritic Cells into Medicine. *Nature* 449, 419–426. doi:10.1038/nature06175
- Sun, J., Zhao, T., Zhao, D., Qi, X., Bao, X., Shi, R., et al. (2020). Development and Validation of a Hypoxia-Related Gene Signature to Predict Overall Survival in Early-Stage Lung Adenocarcinoma Patients. *Ther. Adv. Med. Oncol.* 12, 1758835920937904. doi:10.1177/1758835920937904
- Terry, S., Abdou, A., Engelsens, A. S. T., Buart, S., Dessen, P., Corgnac, S., et al. (2019). AXL Targeting Overcomes Human Lung Cancer Cell Resistance to NK- and CTL-Mediated Cytotoxicity. *Cancer Immunol. Res.* 7 (11), 1789–1802. doi:10.1158/2326-6066.cir-18-0903
- Tran Janco, J. M., Lamichhane, P., Karyampudi, L., and Knutson, K. L. (2015). Tumor-infiltrating Dendritic Cells in Cancer Pathogenesis. *J. Immunol.* 194 (7), 2985–2991. doi:10.4049/jimmunol.1403134
- Tu, L., Guan, R., Yang, H., Zhou, Y., Hong, W., Ma, L., et al. (2020). Assessment of the Expression of the Immune Checkpoint Molecules PD-1, CTLA4, TIM-3 and LAG-3 across Different Cancers in Relation to Treatment Response, Tumor-Infiltrating Immune Cells and Survival. *Int. J. Cancer* 147 (2), 423–439. doi:10.1002/ijc.32785
- Vuong, L., Kotecha, R. R., Voss, M. H., and Hakimi, A. A. (2019). Tumor Microenvironment Dynamics in Clear-Cell Renal Cell Carcinoma. *Cancer Discov.* 9 (10), 1349–1357. doi:10.1158/2159-8290.cd-19-0499
- Wang, C., Thudium, K. B., Han, M., Wang, X.-T., Huang, H., Feingersh, D., et al. (2014). *In Vitro* characterization of the Anti-PD-1 Antibody Nivolumab, BMS-936558, and *In Vivo* Toxicology in Non-human Primates. *Cancer Immunol. Res.* 2 (9), 846–856. doi:10.1158/2326-6066.cir-14-0040
- Wang, Y., Du, L., Yang, X., Li, J., Li, P., Zhao, Y., et al. (2020). A Nomogram Combining Long Non-coding RNA Expression Profiles and Clinical Factors Predicts Survival in Patients with Bladder Cancer. *Aging (Albany NY)* 12 (3), 2857–2879. doi:10.18632/aging.102782
- Wilkerson, M. D., and Hayes, D. N. (2010). ConsensusClusterPlus: a Class Discovery Tool with Confidence Assessments and Item Tracking. *Bioinformatics* 26 (12), 1572–1573. doi:10.1093/bioinformatics/btq170
- Wu, T., and Dai, Y. (2017). Tumor Microenvironment and Therapeutic Response. *Cancer Lett.* 387, 61–68. doi:10.1016/j.canlet.2016.01.043
- Xiong, Y., You, W., Hou, M., Peng, L., Zhou, H., and Fu, Z. (2018). Nomogram Integrating Genomics with Clinicopathologic Features Improves Prognosis Prediction for Colorectal Cancer. *Mol. Cancer Res.* 16 (9), 1373–1384. doi:10.1158/1541-7786.mcr-18-0063
- Yang, L., Shen, M., Xu, L. J., Yang, X., Tsai, Y., Keng, P. C., et al. (2017). Enhancing NK Cell-Mediated Cytotoxicity to Cisplatin-Resistant Lung Cancer Cells via MEK/Erk Signaling Inhibition. *Sci. Rep.* 7 (1), 7958. doi:10.1038/s41598-017-08483-z
- Yoshihara, K., Shahmoradgoli, M., Martínez, E., Vegesna, R., Kim, H., Torres-García, W., et al. (2013). Inferring Tumour Purity and Stromal and Immune Cell Admixture from Expression Data. *Nat. Commun.* 4, 2612. doi:10.1038/ncomms3612
- Zhang, C., He, H., Hu, X., Liu, A., Huang, D., Xu, Y., et al. (2019). Development and Validation of a Metastasis-Associated Prognostic Signature Based on Single-Cell RNA-Seq in clear Cell Renal Cell Carcinoma. *Aging (Albany NY)* 11 (22), 10183–10202. doi:10.18632/aging.102434

**Conflict of Interest:** The authors declare that the research was conducted in the absence of any commercial or financial relationships that could be construed as a potential conflict of interest.

**Publisher's Note:** All claims expressed in this article are solely those of the authors and do not necessarily represent those of their affiliated organizations or those of the publisher, the editors, and the reviewers. Any product that may be evaluated in this article or claim that may be made by its manufacturer is not guaranteed or endorsed by the publisher.

Copyright © 2021 Zhang, Li, Zhang, Wang, Yang, Shao, Liang, Ma, Zhang, Jing, Song and Fan. This is an open-access article distributed under the terms of the Creative Commons Attribution License (CC BY). The use, distribution or reproduction in other forums is permitted, provided the original author(s) and the copyright owner(s) are credited and that the original publication in this journal is cited, in accordance with accepted academic practice. No use, distribution or reproduction is permitted which does not comply with these terms.